Laser site-selective excitation spectroscopy of Eu^{3+}-doped yttrium aluminum garnet

YongRong Shen,[1,2] ChunMao Li,[3] Vilma C. Costa,[1] and Kevin L. Bray[2]
[1]*Department of Chemistry, Washington State University, Pullman, Washington 99164-4630*
[2]*Department of Physics and Astronomy, University of Georgia, Athens, Georgia 30460-2451*
[3]*Jiangsu Engineering Consulting Center, Nanjing 210003, People's Republic of China*
(Received 10 February 2003; revised manuscript received 25 April 2003; published 3 July 2003)

We report the results for laser site selective excitation spectroscopy of Eu^{3+}-doped yttrium aluminum garnet. We identified four primary luminescent centers (A–D) from the $^7F_0 \rightarrow {}^5D_0$ excitation spectra and, from the $^5D_0 \rightarrow {}^7F_1$ luminescence spectra, further identified five, two, four, and two secondary centers, respectively, within these primary A–D centers. From a detailed investigation of their spectroscopic properties that specifically include the $^5D_0$ energy (E_0), the $^5D_0$ lifetime (τ_0), and the crystal-field strength ($S_k, k=2,4,6$), we found trends of E_0 in $E_0(\mathrm{A}) < E_0(\mathrm{B}) < E_0(\mathrm{C}) < E_0(\mathrm{D})$, τ_0 in $\tau_0(\mathrm{A}) > \tau_0(\mathrm{B}) > \tau_0(\mathrm{C}) > \tau_0(\mathrm{D})$, and S_2 in $S_2(\mathrm{A}) < S_2(\mathrm{B}) < S_2(\mathrm{C}) < S_2(\mathrm{D})$. Local structures of the four primary Eu^{3+} centers were proposed. The A center is attributed to regular, unperturbed $Eu^{3+}(c)$ ions and the other three B–D centers are attributed to $Eu^{3+}(c)$ ions perturbed by the next-nearest neighbor $Y^{3+}(a)$ ions that are created by a site exchange between $Y^{3+}(c)$ and $Al^{3+}(a)$ cations during crystal growing. The secondary centers' local structures were also proposed. They form due to a further perturbation of the next-nearest neighbor $Eu^{3+}(c)$ or $Al^{3+}(c)$ ions on each of the primary centers.

DOI: 10.1103/PhysRevB.68.014101 PACS number(s): 78.55.Hx, 71.70.Ch, 42.70.Hj, 61.72.−y

I. INTRODUCTION

The demands for tunable solid-state lasers over a wide spectral range from the ultraviolet to the infrared and for new types of compact high-power laser systems using red or near-infrared laser diode pumping devices[1–4] have stimulated further increased interest in the development and research of rare earth activated laser materials. A wide family of cubic garnets ($Ia3d$ space group) having a general form $C_3A_2D_3O_{12}$, where C denotes the dodecahedral c sites (D_2 local symmetry), A the octahedral a sites (C_{3i}), and D the tetrahedral d sites (S_4) in the garnet lattice, are promising laser host materials of rare earth and transition metal lasing active ions because of their wide transparency, high optical damage threshold, and good thermoconductivity. The $C(c)$ sites are occupied by rare earth ions such as Y^{3+}, Gd^{3+}, La^{3+}, or Lu^{3+}, the $A(a)$ sites by Al^{3+}, Ga^{3+}, or Sc^{3+}, and the $D(d)$ sites by Al^{3+} or Ga^{3+}.

Numerous spectroscopy studies of trivalent rare earth ions (Re^{3+}) in garnets have shown a multisite feature of Re^{3+} in the host lattice.[5–11] The presence of structural defects or impurities in the vicinity of Re^{3+} dopants could modify the local crystal-field symmetry and strength that lead to a variety of nonequivalent Re^{3+} centers. The nonequivalent Re^{3+} centers can exhibit distinct luminescence properties that include energies of energy levels, oscillator strengths, and electron-lattice couplings.

In an early review article,[12] Osiko *et al.* in 1984 reported that high temperature (HT) Czochralski-grown garnet crystals slightly deviate from stoichiometry toward an excess of C_2O_3. Thus, excessive C cations would occupy the a sites. They summarily reported that Re^{3+} dopant ions in HT-grown garnet systems can exist in three major residing forms: i) regular $Re^{3+}(c)$ sites, (ii) perturbed $Re^{3+}(c)$ sites by adjacent $C(a)$ cations, and (iii) paired $Re^{3+}(c)$–$Re^{3+}(c)$ sites. The investigation of Re^{3+} multisite structures is important for elucidation of structural defects and for mechanisms of Re^{3+}–Re^{3+} interactions or Re^{3+}-defect interactions that lead to quenching of luminescence and degradation of lasing. To date, however, no definite correlation between the luminescent Re^{3+} centers and their local structures are established because of the complexity of absorption and luminescence spectra of mostly studied Re^{3+} ions such as Nd^{3+}, Er^{3+}, and Pr^{3+} ions.[8,10–12]

In this study, we have considered a Eu^{3+} dopant ion as a structural probe to resolve the multisites of rare earth ions as lasing centers that always exist in garnet host materials and have the strong influence on the performance of lasing because it possesses both a non-degenerate $^7F_0$ ground state and a non-degenerate $^5D_0$ excited state (Fig. 1). The $^7F_0 \leftrightarrow {}^5D_0$ transition that is a spectral singlet system permits an unambiguous deconvolution of Eu^{3+} multisites directly

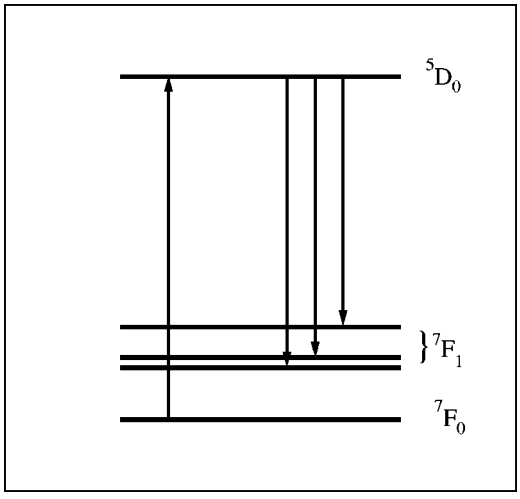

FIG. 1. Simplified energy level diagram of YAG:Eu^{3+}.

through the number of spectral lines appearing in the spectrum. This transition has been used widely and successfully as spectroscopic probes for biological studies,[13] and as structural probes for phase transition studies of materials,[14] and for thermodynamic studies of solutions.[15,16] A simple model system (Fig. 1) consisting of a $^7F_0 \rightarrow {}^5D_0$ excitation transition and $^5D_0 \rightarrow {}^7F_1$ luminescence transitions of Eu^{3+} in $Y_3Al_5O_{12}$ (YAG) (yttrium aluminum garnet) has been proposed and experimentally a laser site selective excitation technique has been used to identify and resolve multisites of YAG:Eu^{3+}. The $^7F_1$ crystal-field splittings have also provided additional insights into the crystal-field symmetry and strength of YAG:Eu^{3+}. This has therefore provided the opportunity for us to study and establish a definite relation between the luminescent centers and their local structures.

II. EXPERIMENT

Laser selective excitation measurements were performed with a pulsed spectroscopy setup. The setup consisted of a pulsed dye laser (Spectra-Physics PDL-3) pumped with a *Q*-switched YAG:Nd^{3+} laser (Continuum NY-61), a 1 m monochromator (Spex 1704/2), and a photon counting detection system. A 60:40 mixture of 590 and 560 rhodamine dyes provided a 570–583-nm tunable range and the dye laser provided a laser line width of approximately 0.01 nm. Nonselective broadband excitation luminescence was excited with a 100 W tungsten-halogen lamp (PBI QH-100) equipped with a dielectric filter passing all wavelengths shorter than 500 nm. Luminescence decays were collected by sending the photomultiplier tube signal directly to a digital storage oscilloscope (LeCroy 140) equipped with a 10 kΩ load resistor. The samples were cooled down to 12 K by a closed-cycle helium refrigerator (APD Cryogenics, Model CSW-204SL).

The nominally 0.1 wt% Eu^{3+}-doped YAG single crystal samples used for this study were grown using the HT-grown technique and were kindly provided by the Institute for Laser Physics of the University of Hamburger.

III. RESULTS

A. Nonselective broadband excitation

Figure 2 shows a $^5D_0 \rightarrow {}^7F_1$ luminescence spectrum of YAG:Eu^{3+} at 12 K upon non-selective broadband excitation ($\lambda_{ex} < 500$ nm). The spectrum consisted of three strong lines surrounding 590.6, 591.4, and 596.3 nm, which are attributed to three transitions from the nondegenerate $^5D_0$ state to three crystal-field levels of the $^7F_1$ multiplet (Fig. 1). Additionally, we observed several weak lines around the three dominant lines in the spectrum.

B. Laser site selective excitation and luminescence

By monitoring all the luminescence lines appeared in the spectrum upon the non-selective excitation (Fig. 2), we measured $^7F_0 \rightarrow {}^5D_0$ excitation spectra of YAG:Eu^{3+} at 12 K. We observed four different excitation lines (580.93, 580.80, 580.70, and 580.44 nm). Representative excitation spectra monitoring 590.63, 591.50, 589.93, and 590.89 nm luminescence lines are shown in Fig. 3. The four $^7F_0 \rightarrow {}^5D_0$ excitation lines are straightforward attributed to four distinct luminescent centers of Eu^{3+} in YAG (labeled by A, B, C, and D in an ascending order of the $^5D_0$ energy) because the $^5D_0$ excited and $^7F_0$ ground states of Eu^{3+} are nondegenerate.

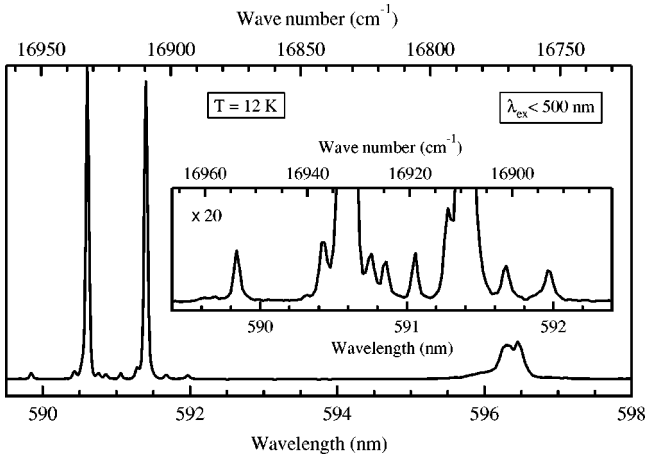

FIG. 2. $^5D_0 \rightarrow {}^7F_1$ luminescence spectrum of YAG:Eu^{3+} at 12 K upon broadband non-selective excitation ($\lambda_{ex} < 500$ nm).

Upon laser selective excitations at $\lambda_{ex} = 580.93$, 580.80, 580.70, and 580.44 nm, we obtained corresponding $^5D_0 \rightarrow {}^7F_1$ luminescence spectra of the four A–D Eu^{3+} centers in YAG (Fig. 4). We clearly notice from Fig. 4 that center D exhibited a simple three line spectral pattern that fits the prediction of the D_2 site symmetry, whereas centers A, B, and C exhibited complicated spectral patterns. In order further to identify and understand the appearance of the complicated spectral patterns, additional higher resolution spectroscopy experiments were performed by tuning a small range of $\Delta\lambda_{ex} = \pm$ 0.02 nm around the individual excitation line peaks of the A–D centers. Figures 5 and 6, as examples, present the results for centers A and C. We observed five, two, four, and two subgroups of satellite lines for centers A–D, respectively. These subgroups of sat-

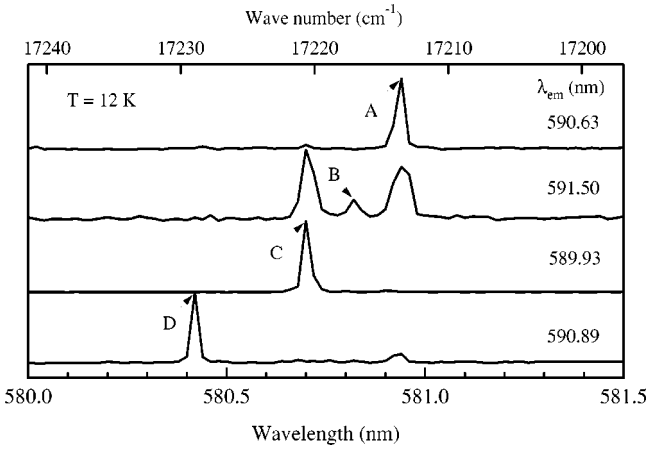

FIG. 3. $^7F_0 \rightarrow {}^5D_0$ excitation spectra of YAG:Eu^{3+} at 12 K by monitoring $\lambda_{em} = 590.63$, 591.50, 589.93, and 590.89 nm luminescence lines. The relative intensities for excitation lines A–D are 1, ~0.60, ~3.52, and ~0.23, respectively.

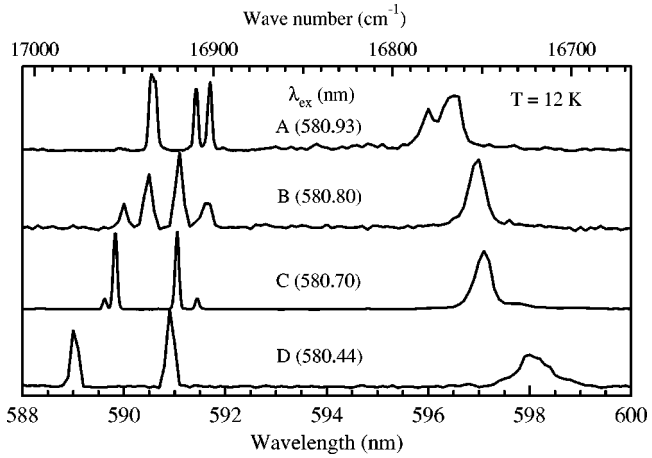

FIG. 4. $^5D_0 \rightarrow {}^7F_1$ luminescence spectra of YAG:Eu^{3+} at 12 K upon four selective excitations at $\lambda_{ex}=580.93$, 580.80, 580.70, and 580.44 nm. The relative intensities for centers A–D are 1, ~0.60, ~3.73, and ~0.21, respectively.

ellite lines are attributed to secondary luminescent centers of each of the primary A-D centers. Line positions of the $^5D_0 \rightarrow {}^7F_1$ luminescence and the $^7F_0 \rightarrow {}^5D_0$ excitation for the primary and secondary centers of YAG:Eu^{3+} are collected in Table I.

C. Annealing treatment experiments

A series of annealing treatment experiments up to 800 °C in three steps of 400, 600, and 800 °C revealed no significant changes in the excitation and luminescence spectra of YAG:Eu^{3+}. This suggests that the primary and secondary luminescent Eu^{3+} centers are not associated with local strains or vacancies created during the crystal growth.

D. Temperature dependence of luminescence and lifetime

We performed temperature dependent luminescence and lifetime measurements between 12 K and room temperature

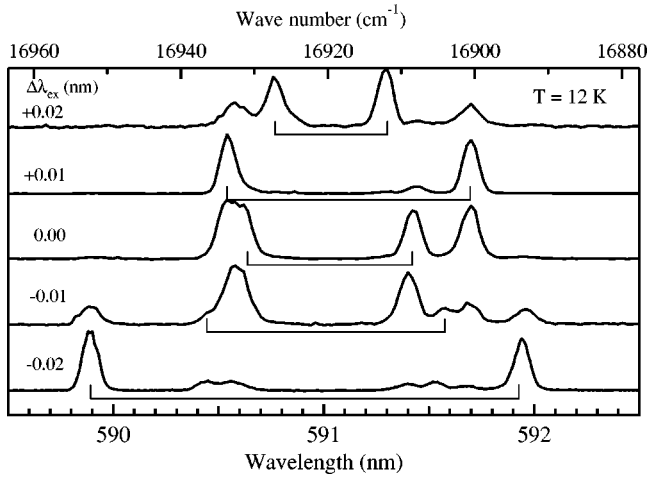

FIG. 5. $^5D_0 \rightarrow {}^7F_1$ luminescence spectra of center A in YAG:Eu^{3+} at 12 K upon $^7F_0 \rightarrow {}^5D_0$ excitations at $\lambda_{ex}=580.93+\Delta\lambda_{ex}$, where $\Delta_{ex}=0$, ± 0.01, and ± 0.02 nm. The relative intensities are 1, ~0.6, ~0.45 for $\Delta_{ex}=0$, ± 0.01, and ± 0.02, respectively.

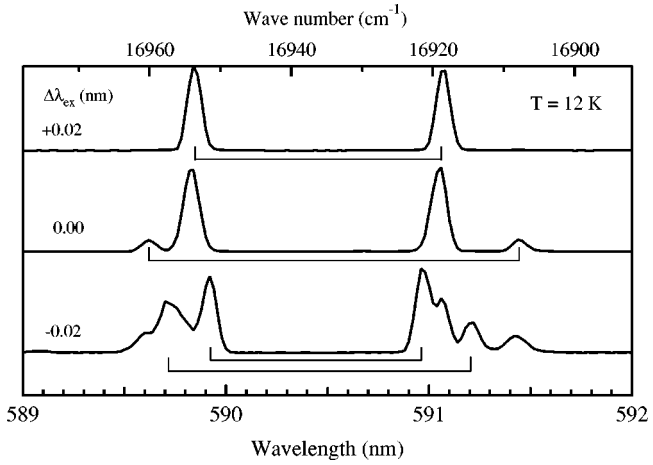

FIG. 6. $^5D_0 \rightarrow {}^7F_1$ luminescence spectra of center C in YAG:Eu^{3+} at 12 K upon $^7F_0 \rightarrow {}^5D_0$ excitations at $\lambda_{ex}=580.70+\Delta_{ex}$, where $\Delta_{ex}=0$ and ± 0.02 nm. The relative intensities are 1 and ~0.30 for $\Delta_{ex}=0$ and ± 0.02 nm, respectively.

(RT). The B and D centers exhibited a gradual quenching in intensity with increasing temperature and a complete quenching above ~250 K. With increasing temperature, the luminescence of the A and C centers was gradually developed to a three line pattern (labeled by asterisks in Table I) and their RT luminescence spectra are shown in Fig. 7(b). In RT excitation experiments, additionally we observed that the A center gradually lost its characteristic $^7F_0 \rightarrow {}^5D_0$ excitation and exhibited strong phonon sidebands in its excitation spectrum [Fig. 7(a)]. Since the excitation spectrum of the A center develops to the broad excitation bands with increasing temperature to RT and the A center loses its own selective excitation character, we also observed a strong luminescence [labeled by asterisks in Fig. 7(b)] from the A center upon excitation at the excitation peak of the C center ($\lambda_{ex}=580.52$ nm at RT).

From variable temperature luminescence decay measurements between 12 K and RT, we obtained 12-K lifetimes of ~3.8, ~3.7, ~3.6, and ~3.4 ms for centers A, B, C, and D, respectively (Fig. 8). Additionally, we observed that the lifetime remained constant between 12 K – RT for center A and between 12 and 200 K for center B, and that the lifetime decreased from 3.6 ms below 150 K to ~3.4 ms at RT for center C and from 3.4 ms below 100 K to ~3.0 ms at 200 K for center D.

IV. DISCUSSION

A. Crystal-field analysis

Energies of three $^7F_1$ crystal-field levels can be determined by an energetic difference between the $^7F_0 \rightarrow {}^5D_0$ excitation transition and three individual $^5D_0 \rightarrow {}^7F_1$ luminescence transitions (Table I) and are presented in Table I. When a Re^{3+} ion is embedded in a host material, it experiences a crystal-field from its neighbor ligands of the host lattice. The crystal-field potential (V_{CF}) is described in a general form[17]

TABLE I. Line positions (nm) of the $^5D_0 \rightarrow {}^7F_1$ luminescence and $^7F_0 \rightarrow {}^5D_0$ excitation of YAG:Eu^{3+} at 12 K, the $^7F_1$ energies $E(\mathrm{cm}^{-1})$, the CF parameters B_{kq} (cm^{-1}), and the CF strength $S_k(\mathrm{cm}^{-1})$. $\overline{S_k}$ denotes the average CF strength. Asterisked positions correspond to the luminescence lines of YAG:Eu^{3+} at RT and slightly shifted to longer wavelength with temperature (<0.1 nm from 12 K to RT).

Center	$^7F_0 \rightarrow {}^5D_0$ (nm)	$^5D_0 \rightarrow {}^7F_1$ (nm)	$E(^7F_1)$ (cm^{-1})	B_{20} (cm^{-1})	B_{22} (cm^{-1})	S_2 (cm^{-1})	$\overline{S_2}$ (cm^{-1})
		589.89	261.8				
		591.94	320.5				
	580.92	5965.1	449.9	529	120	242	
		590.44	277.6				
		591.53	308.8				
	580.92	595.99	435.3	474	64	214	
		590.60*	281.8				
		591.40*	304.7				
	580.93	596.47*	448.5	518	48	233	
		590.55	279.8				
		591.70	312.7				
	580.95	595.92	432.4	454	67	205	
		590.77	285.8				
		591.29	300.7				
A	580.96	596.44	446.7	512	31	229	225
		590.32	277.7				
		590.93	295.2				
	580.80	596.82	462.2	586	36	263	
		589.83	263.3				
		591.47	310.3				
B	580.81	596.80	461.3	582	96	264	263
		589.92	269.7				
		590.97	299.9				
	580.68	596.91	468.2	611	62	275	
		589.71	263.7				
		591.21	306.7				
	580.68	596.58	459.0	580	88	263	
		589.61*	260.2				
		591.44*	312.7				
	580.70	596.58*	458.4	573	107	261	
		589.81	265.4				
		591.06	301.2				
C	580.72	596.93	467.6	614	73	276	269
		588.80	245.2				
		590.77	301.8				
	580.42	597.82	501.5	760	116	344	
		588.88	246.3				
		590.77	300.7				
D	580.46	597.86	501.4	756	111	342	343

$$V_{\mathrm{CF}} = \sum_{k=2,4,6} \sum_{q=-k}^{+k} B_{kq} C_{kq}, \qquad (1)$$

where B_{kq} and C_{kq} are referred to as the crystal-field parameters and electronic angular operators, respectively. The crystal-field strength (S_k) experienced by Re^{3+} ions can be defined as

$$S_k = \left(\frac{1}{2k+1} \sum_{q=-k}^{+k} |B_{kq}|^2 \right)^{1/2}, \quad \text{with } k = 2,4,6. \qquad (2)$$

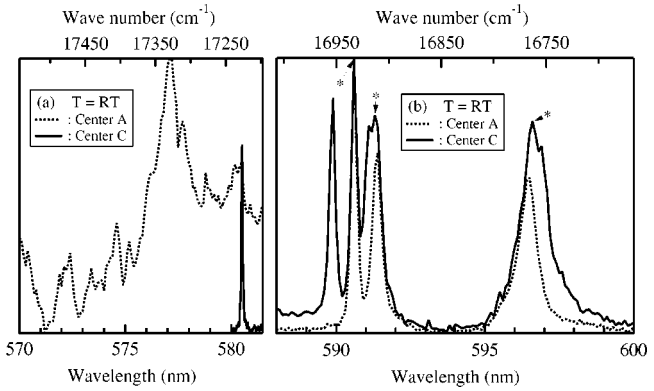

FIG. 7. (a) Room temperature $^7F_0 \rightarrow {}^5D_0$ excitation spectra by monitoring $\lambda_{em}=590.61$ nm for center A and $\lambda_{em}=589.89$ nm for center C; (b) RT $^5D_0 \rightarrow {}^7F_1$ luminescence spectra upon excitation at $\lambda_{ex}=577.10$ nm for center A and $\lambda_{ex}=580.52$ nm for center C. The lines labeled by asterisks belong to the A center.

When Eq. (1) is applied to the $^7F_1$ multiplet of Eu^{3+} substituted at regular $Y^{3+}(c)$ sites (D_2 site symmetry) in YAG, it becomes a simple form as below, when no J mixing is considered:

$$V_{CF}=B_{20}C_{20}+B_{22}C_{22}. \tag{3}$$

Since three $^7F_1$ crystal-field levels can provide two $^7F_1$ crystal-field splittings, two crystal-field parameters (B_{20} and B_{22}) can be exactly calculated by Eq. (3). Calculated values for the B_{20} and B_{22} parameters are given in Table I. The crystal-field strengths (S_2) are readily calculated by Eq. (2) and also included in Table I. For a direct comparison among the primary centers, we averaged the crystal-field strengths over the secondary centers within each of the primary centers. We obtained that the A center experiences a weak crystal-field field, the B and C centers experience an intermediate crystal-field field, and the D center experiences a strong crystal-field field (Table I).

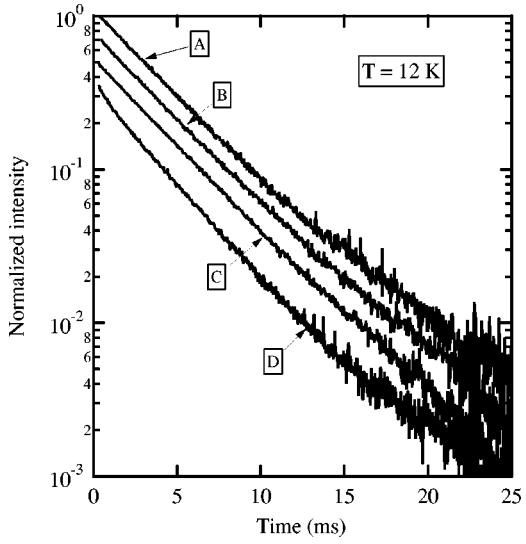

FIG. 8. Luminescence decays of YAG:Eu^{3+} at 12 K.

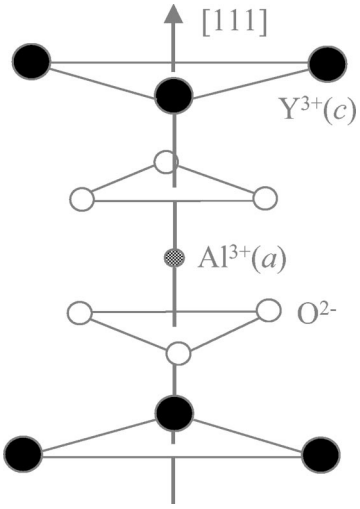

FIG. 9. Local structure of Al(a) cations in YAG along the [111] direction.

B. Local structures of luminescent centers

Chenavas *et al.*[18] in 1978 studied x-ray diffractions of natural, HT-grown, and flux-grown garnet crystals such as $Gd_3Ga_5O_{12}$, $Gd_3Fe_5O_{12}$, and $Y_3Fe_5O_{12}$ and observed {222} reflections in all the crystal samples. The occurrence of the cubic-forbiden {222} reflections indicates a trigonal deviation from the regular rcubic garnet lattice. They proposed a $Ia3d \rightarrow R\bar{3}$ structural deviation in garnet material systems. Lupei *et al.*[11] in 1995 observed the {222} reflections with comparable intensities relative to the cubic-allowed reflections in HT-grown YAG crystals.

Dong and Lu[19] in 1991 used an extended x-ray absorption fine structure (EXAFS) spectroscopy technique to investigate several garnet crystals such as $Y_3Fe_5O_{12}$, $Gd_3Ga_5O_{12}$, $Y_3Ga_5O_{12}$, $Y_3Al_5O_{12}$, and $Er_3Al_5O_{12}$ and to observe a site exchange between C and A cations. They quantitatively estimated that about two C cations exchange their c sites with two A cations at the a sites per unit cell and proposed that such a site exchange leads to the structural distortion from the cubic ($Ia3d$) to the trigonal ($R\bar{3}$).

Unavoidable displacements of cationic positions accompany the site exchanges between the C and A cations due to the difference in their cationic radii. In YAG, each $Al^{3+}(a)$ cation is surrounded by six next-nearest neighbor (NN) $Y^{3+}(c)$ cations (Fig. 9). Significant displacements of $Y^{3+}(a)$ cations along the [111] direction occur due to a large difference in Y^{3+} and Al^{3+}) cationic radii ($\sim$1.02 Å for Y^{3+} and $\sim$0.53 Å for Al^{3+}) and, as a consequence, lead to three possible non-equivalent perturbations at the NN c sites when the inversion symmetry around the central a site is preserved (Fig. 9).

Based on the above-aforesaid x-ray diffraction and EXAFS studies,[11,19] we therefore attribute the four primary Eu^{3+} centers observed in YAG:Eu^{3+} to Eu^{3+} ions at a regular, unperturbed c site and at three non-equivalently perturbed c sites by the NN $Y^{3+}(a)$ ions. We further expect that the primary A center is associated with Eu^{3+} ions at the unperturbed c sites based on the fact that the A center exhib-

ited the predominant luminescence under the non-selective excitation (Fig. 2), the lowest energy of the $^5D_0$ excited state (Fig. 3 and Table I), and the presence of the strong phonon sidebands in the $^7F_0 \rightarrow {}^5D_0$ excitation transition (Fig. 7). Based on the trends of the $^5D_0$ energy (E_0) in $\underline{E_0}$(D) $>\underline{E_0}$(C) $>\underline{E_0}$(B) and of the crystal-field strength in $\underline{S_2}$(D) $>S_2$(C) $>S_2$(B), we also expect that the primary B–D centers are associated with three nonequivalent NN $Eu^{3+}(c)$–$Y^{3+}(a)$ ion pairs with long, intermediate, and short interionic distances between $Eu^{3+}(c)$ and $Y^{3+}(a)$, respectively. We can attribute the secondary centers observed in each of the primary A–D centers to the regular $Eu^{3+}(c)$ sites and the three distinct $Y^{3+}(a)$-associated $Eu^{3+}(c)$ sites perturbed further by NN $Eu^{3+}(c)$ or $Al^{3+}(c)$ ions.

V. CONCLUSIONS

From a detailed analysis of the laser site selective excitation spectroscopy in YAG:Eu^{3+}, we have identified four primary luminescent centers (A–D) and several secondary luminescent centers within each of the primary centers.

The primary A center exhibited a predominant luminescence under the non-selective broadband excitation and strong phonon sidebands in the $^7F_0 \rightarrow {}^5D_0$ excitation transition. This center possesses the lowest energy of the $^5D_0$ excited state, the long $^5D_0$ lifetime, and the weakest crystal-field (CF) strength. We attribute the A center to Eu^{3+} ions at unperturbed $Y^{3+}(c)$ sites with the regular site symmetry (D_2). The other primary B–D centers showed the spectroscopic properties, specifically, for the $^5D_0$ energy in E_0(B) $<E_0$(C) $<E_0$(D), the $^5D_0$ lifetime in $\underline{\tau_0}$(B) $>\underline{\tau_0}$(C) $>\underline{\tau_0}$(D), and the crystal-field strength in $\underline{S_2}$(B) $<\underline{S_2}$(C) $<S_2$(D). These spectroscopic properties have been used in conjunction with the previous x-ray structural and extended x-ray absorption fine structure spectroscopic studies[11,18,19] to propose that the primary B–D centers are three nonequivalent $Eu^{3+}(c)$–$Y^{3+}(a)$ ion pairs.

ACKNOWLEDGMENTS

We gratefully acknowledge financial support from the U.S. National Science Foundation through Grant No. DMR-0107802. V.C.C. also acknowledges financial support from Brazilian National Council of Research, CNPq. We thank Professor Günter Huber at the Institute for Laser Physics of the University of Hamburger for supplying the samples used for this study.

[1] S. Kück, Appl. Phys. B: Photophys. Laser Chem. **72**, 515 (2001).
[2] D. W. Chen, C. L. Fincher, T. S. Rose, F. L. Vernon, and R. A. Fields, Opt. Lett. **24**, 385 (1999).
[3] A. Diening and S. Kück, J. Appl. Phys. **87**, 4063 (2000).
[4] S. Konno, S. Fujikawa, and K. Yasui, Appl. Phys. Lett. **70**, 2650 (1997).
[5] Y. K. Voronko and A. A. Sobol, Phys. Status Solidi A **27**, 257 (1975).
[6] M. K. Ashurov, Y. K. Vornko, V. V. Osiko, A. A. Sobol, and M. I. Timoshechkin, Phys. Status Solidi A **42**, 101 (1977).
[7] M. Asano and J. A. Koningstein, Chem. Phys. **42**, 369 (1979).
[8] M. Malinowski, P. Szczepanski, W. Wolinski, R. Wolski, and Z. Frukacz, J. Phys.: Condens. Matter **5**, 6469 (1993).
[9] E. Antic-Fidancev, M. Lemaitre-Blaise, and P. Porcher, J. Alloys Compd. **207/208**, 90 (1994).
[10] A. Lupei, H. Gross, and P. Reiche, J. Phys.: Condens. Matter **7**, 5701 (1995).
[11] V. Lupei, A. Lupei, C. Tiseanu, S. Georgescu, C. Stoicescu, and P. M. Nanau, Phys. Rev. B **51**, 8 (1995).
[12] V. V. Osiko, Y. K. Voron'ko, and A. A. Sobol, in *10 Crystals — Growth, Properties, and Applications*, edited by H. C. Freyhardt *et al.* (Springer-Verlag, Berlin, 1984), pp. 38–86.
[13] J.-C. Bunzli and G. Choppin, *Lanthanide Probes in Life, Chemical, and Earth Sciences* (Elsevier, New York, 1989).
[14] J. R. Peterson, J. Alloys Compd. **225**, 11 (1995).
[15] M. F. Yeh, T. Riedener, K. L. Bray, and S. B. Clark, J. Alloys Compd. **303/304**, 37 (2000).
[16] C. L. Maupin, A. Mondry, L. Leifer, and J. P. Riehl, J. Phys. Chem. A **105**, 3071 (2001).
[17] S. Hüfner, *Optical Spectra of Transparent Rare Earth Compounds* (Academic Press, New York, 1978).
[18] J. Chenavas, J. C. Joubert, and M. Marezio, J. Less-Common Met. **62**, 373 (1978).
[19] J. Dong and K. Q. Lu, Phys. Rev. B **43**, 8808 (1991).